JOURNAL OF MATERIALS SCIENCE 16 (1981) 1567–1578

Temperature–strain rate dependance of compressive strength and damage mechanisms in aluminium oxide

JAMES LANKFORD
Department of Materials Sciences, Southwest Research Institute, San Antonio, Texas 78284, USA

The results of compression tests of Al_3O_3 performed over a wide range of temperatures and strain rates are interpreted in terms of dominant damage mechanisms. It is shown that compressive failure in Al_2O_3 is caused by one of three different mechanisms, each based on tensile (Mode I) growth of predominantly axial microcracks, and each characteristic of a specific temperature–strain rate regime. The concepts developed should be applicable to other strong ceramics.

1. Introduction

Damage caused by compressive loading is an important consideration in a number of technological applications of high-strength ceramics. Such situations arise, for example, during operation of turbines, in which thermal cycle-induced compressive stresses may be produced; in other cases, turbines may be preloaded in compression, to minimize tensile loads. In addition, compressive microfracture probably is an important failure mode during particle impact (erosion) of ceramic radomes, infra-red windows, turbine blades and during wear of ceramic bearing surfaces.

Like tensile fracture, failure under compressive loading has been recognized as a process which is dependent upon both temperature and loading rate. However, it has generally been assumed that tensile and compressive fracture are fundamentally different. The present objective is to bring together the results of an experimental investigation of aluminium oxide which has extended over several years [1, 2], including recent tests carried out at high temperatures and strain rates, and to interpret these results in terms of current failure models. It will be suggested that for strong ceramics like Al_2O_3, both tensile and compressive failure actually occur through basically identical microfracture processes, the principal difference being that compressive failure involves multiple cracks, while tensile fracture occurs through the action of a single dominant crack.

2. Experimental procedure

Specimen preparation and testing procedures have previously been described [1–3]. Briefly, 15.87 mm diameter × 12.5 mm long right circular cylinders of Lucalox polycrystalline α-alumina* (as-fired) were loaded to failure in compression. Experiments were performed at strain rates of 7×10^{-5} and $2 \times 10^{-1}\,sec^{-1}$ using a standard servo-controlled hydraulic test machine, and at $\sim 2 \times 10^{3}\,sec^{-1}$ in a Hopkinson pressure bar. Temperature was varied from 77 to 1800 K; over this range the development of compressive damage was monitored for the lowest strain rate using acoustic emission. Failed specimens were studied fractographically in the scanning electron microscope (SEM). The latter was also used to characterize microscopic compressive damage manifested on the outer surfaces of highly stressed specimens subjected to various temperature–strain rate combinations.

3. Results

3.1. Compression tests

Compressive strength (σ_c) as a function of temperature (T) for all three strain rates ($\dot{\epsilon}$) is shown in Fig. 1, together with the stress level correspond-

*General Electric Lamp Glass Division, Cleveland, Ohio, USA.

0022–2461/81/061567–12$03.20/0

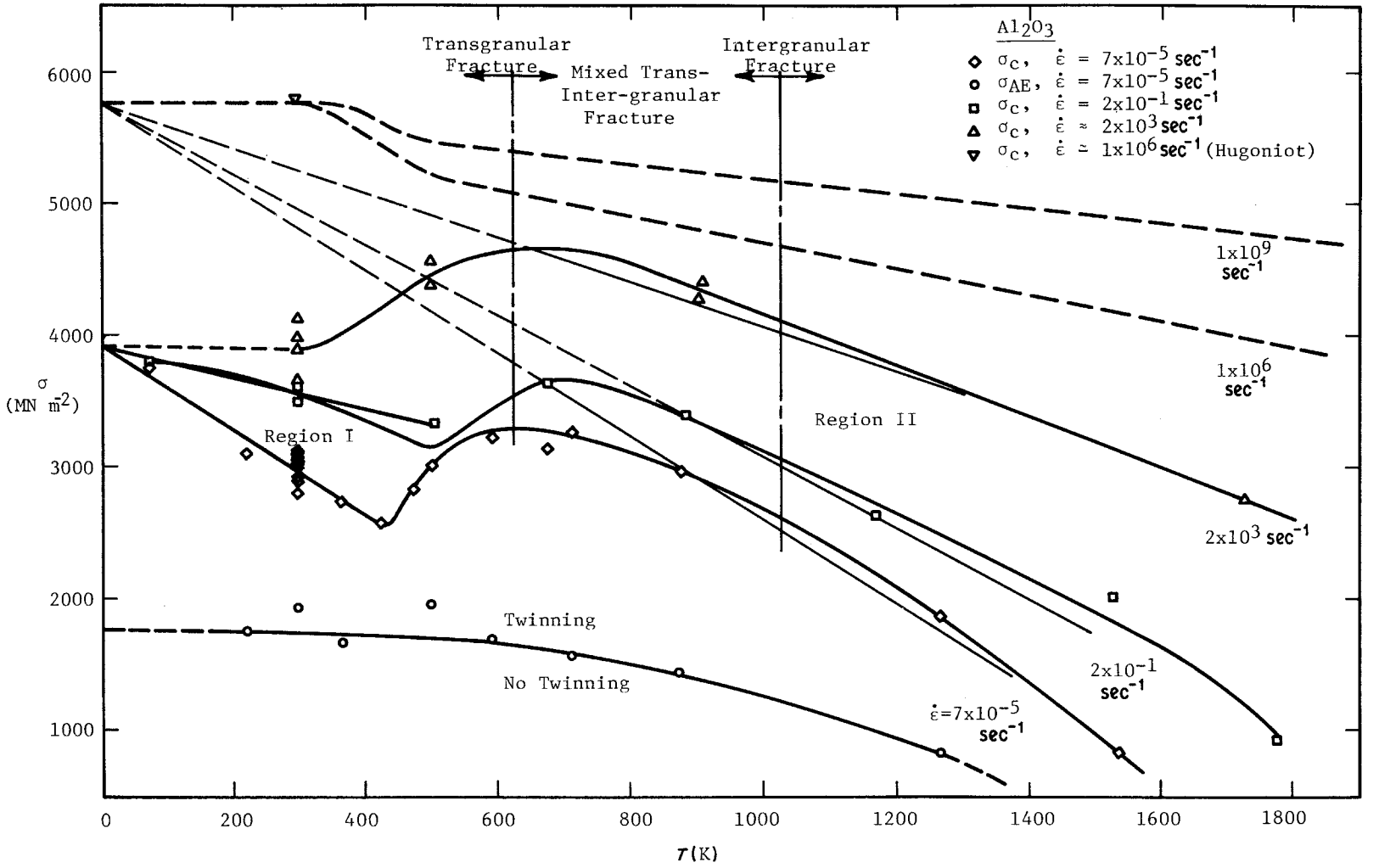

Figure 1 Compressive strength against temperature as a function of strain rate.

ing to the onset of acoustic emission (σ_{AE}). Also shown is a data point (the average of several tests) representing recent Hugoniot shock measurements ($\dot{\epsilon} \gtrsim 10^4\ \mathrm{sec}^{-1}$) carried out by Munson and Lawrence [4] on Lucalox. Of particular interest are the strength increase between 500 and 700 K, the decrease in σ_c and σ_{AE} for $T > 900$ K, and the total suppression of acoustic emission for $T \gtrsim 1300$ K. Linear extrapolation of the low-temperature (Region I) σ_c data shows that they converge at $T = 0$ K to a strength of approximately 4075 MN m^{-2}. Similarly the high-temperature (Region II) results extrapolate to a stress level of 5750 MN m^{-2} at absolute zero. Regions I and II are connected by a transition region, corresponding to a change in fracture mode (discussed shortly).

The low-temperature stress level for twinning was determined by SEM observation. Earlier work [2], reporting an upward trend in σ_{AE} with decreasing T, erred in that the background AE level was too high, owing to liquid nitrogen "noise" (bubbles), thereby masking the true twinning stress threshold. Microscopic inspection indicates that the twinning threshold actually is essentially athermal.

Additional aspects of the experimental results are apparent upon replotting them in the form σ_c against $\log \dot{\epsilon}$, as shown in Fig. 2. Here the Regions I and II data again converge, at $\dot{\epsilon} \cong 10^5$ and $5 \times 10^{12}\ \mathrm{sec}^{-1}$, respectively. However, in the case of the room-temperature Region I plot, there is an abrupt acceleration in the rate of increase in strength with strain rate (Region III), beginning at $\dot{\epsilon} \gtrsim 10^3\ \mathrm{sec}^{-1}$; at this point, the slope of $\sigma_c(\dot{\epsilon})$ increases by more than an order of magnitude, from ~ 0.02 to ~ 0.27.* Finally, by inspection, it is possible to deduce effective strength levels which would be obtained at strain rate levels too high to be achieved in normal controlled tests. This process yields the predicted $\sigma_c(T)$ plots shown in Fig. 1 for $\dot{\epsilon} = 10^6$ and $10^8\ \mathrm{sec}^{-1}$.

Acoustic emission was obtained in terms of total counts (N) in excess of a minimum threshold level against both increasing compressive stress σ and time t. $N(t)$ was differentiated to yield $dN/dt(\sigma)$, as shown in Fig. 3. Also shown is the result of acoustic emission during bending of a ground, hence pre-microcracked, specimen of Lucalox [5]. The first stage (slope $S_1 \doteq 5$) of the compressive $dN/dt(\sigma)$ relationship has been identified [3] with crack nucleation, while the acoustic emission response of the tensile specimen has no such first stage, and has been shown to represent tensile microcrack extension prior to fracture [5].

3.2. Fractographic analysis

The fractographic features associated with failure over a wide temperature range are shown in Fig. 4. At 77 K (Fig. 4a) the failure surface is principally transgranular, with only occasional intergranular features, while at 743 K (Fig. 4b), somewhat more intergranular fracture is present. In both photos, the transgranular regions appear rather smooth, but non-crystallographic. This situation changes as higher temperatures are attained; at 1190 K, for example, the fracture is predominantly intergranular and the relatively few transgranular regions (arrows) differ in appearance from those characteristic of lower temperatures; rather than being flat, they are composed mostly of jagged, straight-edged crystallographic steps (Fig. 4c). At still higher temperatures, fracture is almost entirely intergranular (Fig. 4d, $T = 1560$ K). In fact, fracture is so intergranular that the "dust" to which most of the test specimen is reduced consists of individual, perfect crystallites of sapphire. This is true even for strain rates of the order of $10^3\ \mathrm{sec}^{-1}$, as shown in Fig. 5.

It should be noted that bending (tensile) tests on Lucalox have been carried out [6] at an intermediate loading rate over (essentially) the same temperature range. The fractographic observations made on these specimens were basically identical to those described above for compressive failure.

Further fractographic detail is visible at higher magnification. In Fig. 6, it can be seen that at 900 K, the intergranular facets are almost perfectly smooth and featureless. For $T \gtrsim 1300$ K, on the other hand, careful study shows that for all loading rates, the facets are covered with a multitude of what appear to be the remains of a liquid phase which has agglomerated into solidified globules (Fig. 6a). It should be emphasized that these globules are not fracture debris; each compressive fracture fragment was immersed in alcohol and cleaned ultrasonically prior to coating for SEM study. For tests carried out at $T < 1300$ K, this process produces facets which are perfectly devoid of such globules (Fig. 6b).

*It is possible, of course, that the transition to a higher slope for the Al_2O_3 occurs at a strain rate between 2×10^3 and $1 \times 10^4\ \mathrm{sec}^{-1}$, in which case the slope following the transition would exceed 0.27.

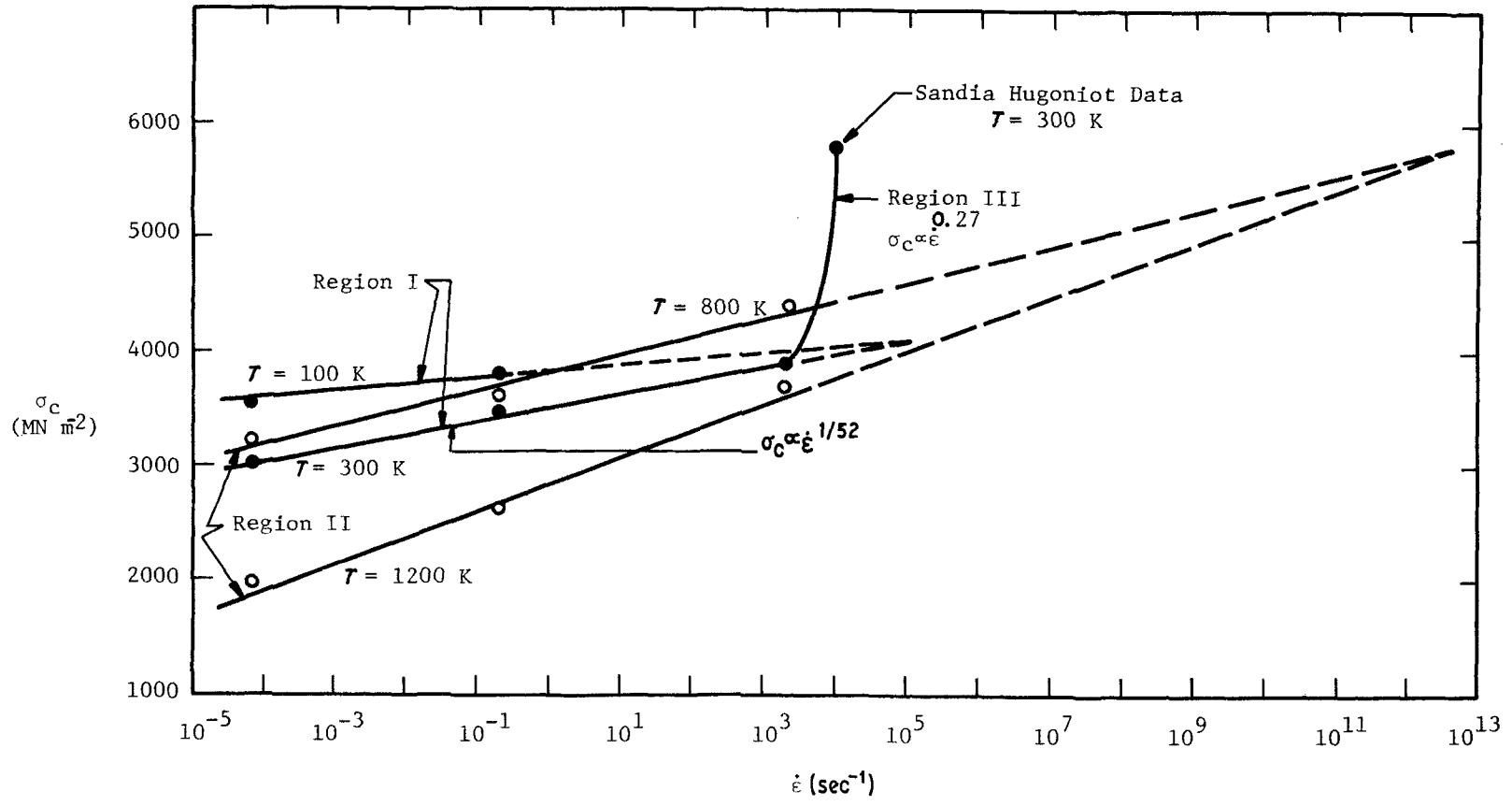

Figure 2 Compressive strength against strain rate as a function of temperature, showing three damage regimes.

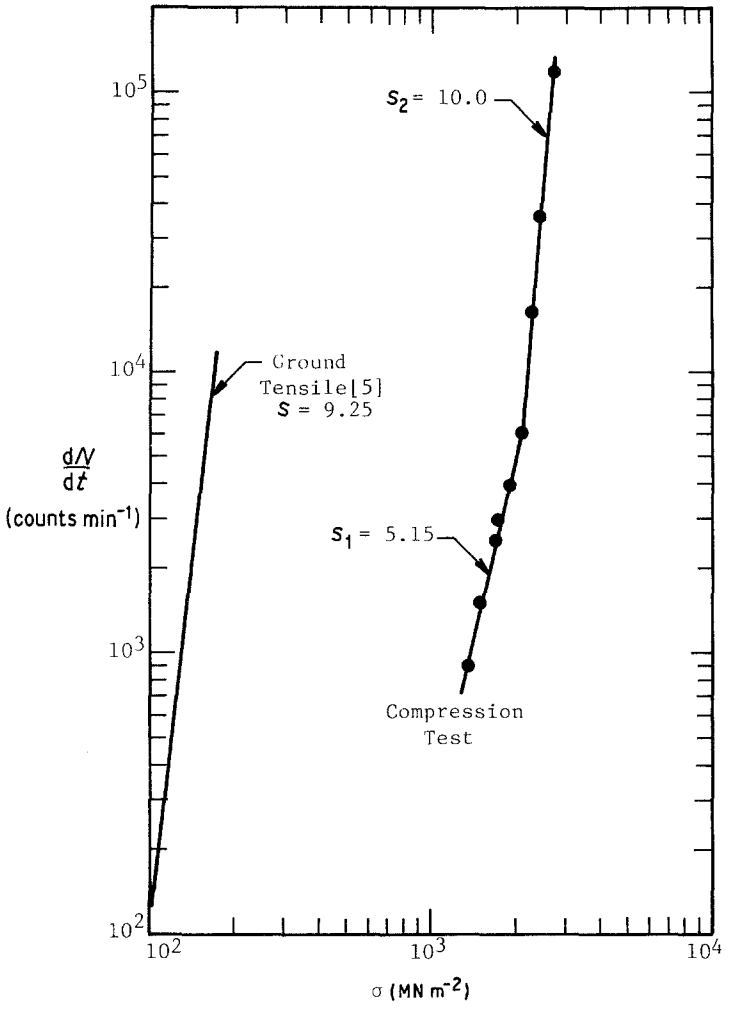

Figure 3 Acoustic emission count rate against applied stress for Lucalox, $T \simeq 300$ K.

3.3. Microplasticity observations

From 77 to ~ 900 K, the only evidence of microplasticity is the formation of twins, as discussed elsewhere [1]. The significance of these twins is that they nucleate microcracks, as shown in Fig. 7, particularly within grains adjacent to grain boundaries impinged upon by twins. Above 900 K, twins still form, but they are now much thicker (Fig. 8a), and have less propensity to form cracks. Twinning cracks which do form are located at the twin–parent interface, rather than being the product of the twin impacting a grain boundary, as is common at lower temperatures. In fact, once the few twin-nucleated microcracks encounter grain boundaries, they change mode to intergranular (Fig. 8b). Generally, higher temperature microcracks form along grain boundaries, often nucleating at the triple points, and remain intergranular as the crack grows (Fig. 8a). Although some evidence of possible dislocation activity was seen, it was not extensive.

It should be noted that the process of microcracking itself represents a form of plasticity. The predominant microcrack orientation observed, regardless of temperature or strain rate, was (near) axial, i.e. the compression axis tended to lie in the plane of the crack.

4. Analysis of damage mechanisms

In the following sections, the compressive failure of Al_2O_3 will be analysed based on the foregoing experimental observations. To simplify the discussion, three regions of failure will be considered, as exemplified in Fig. 2: (1) a thermally activated, low-temperature regime, in which $\dot{\epsilon} \lesssim 10^3\,\text{sec}^{-1}$; (2) a thermally activated, high-temperature regime; (3) a low-temperature regime characterized by $\dot{\epsilon} > 10^3\,\text{sec}^{-1}$ (this regime may extend to high temperatures as well).

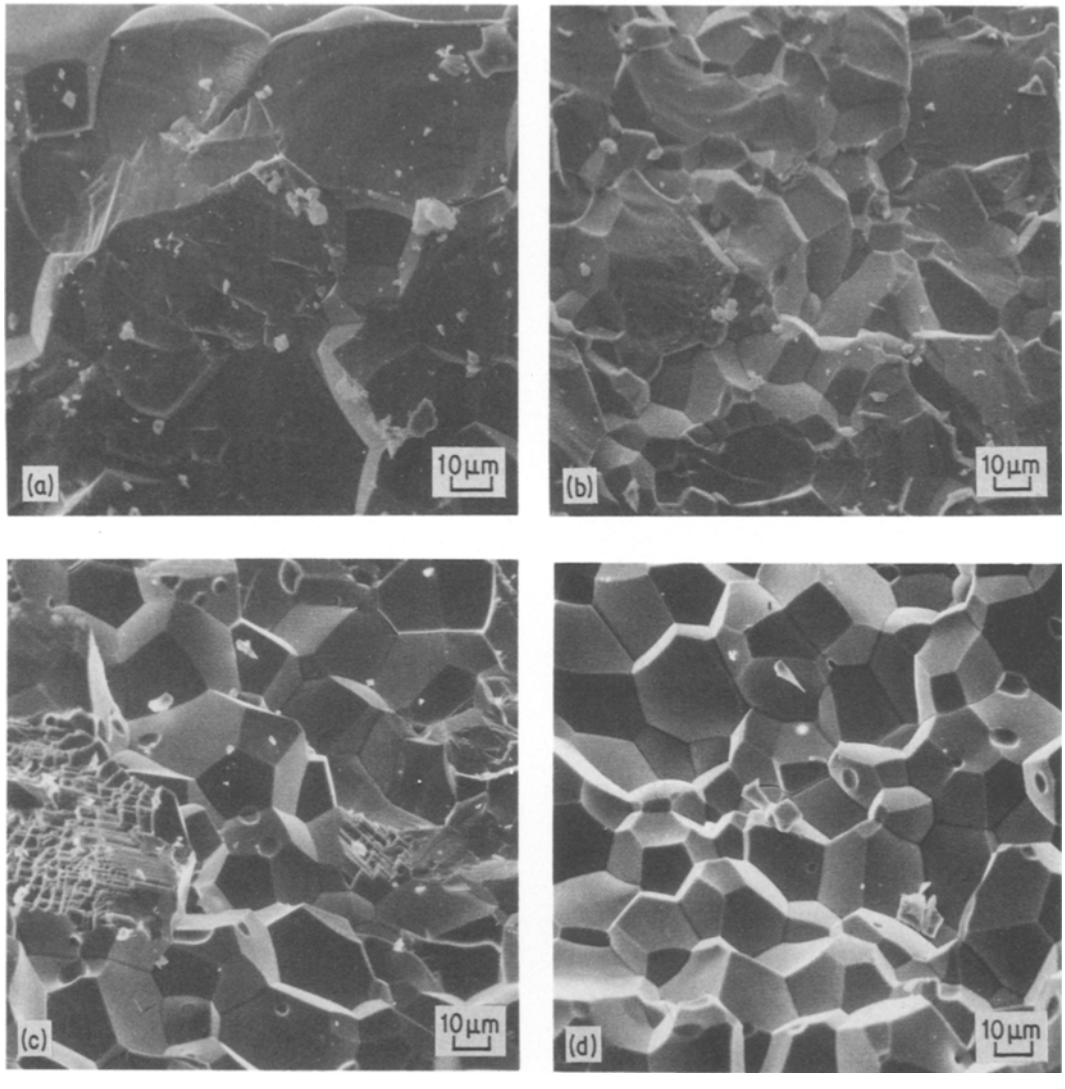

Figure 4 Fracture surfaces for Al_2O_3 failed under compression, $\dot{\epsilon} = 7 \times 10^{-5}\,sec^{-1}$. (a) $T = 77\,K$, (b) $T = 743\,K$, (c) $T = 1190\,K$, (d) $T = 1560\,K$.

4.1. Region 1: $0 \leqslant T \gtrsim 500\,K$, $\dot{\epsilon} \lesssim 10^3\,sec^{-1}$

In this regime, three basic processes appear to cause a specimen to fail, namely, (1) twins nucleate, forming associated axial microcracks, which (2) grow, and eventually (3) coalesce at failure. At least one of these processes must be thermally activated, to account for the observed strain rate–temperature dependence of σ_c.

It is not expected that crack coalescence can account for this effect, since coalescence occurs only in the last instant of compressive failure. Similarly, from the apparent temperature insensitivity (Fig. 1) of the twinning threshold, crack nucleation* does not seem to exhibit the requisite thermally activated character.

Since two of the possibilities can be minimized, it therefore seems necessary to consider first whether axial cracks in uniaxial compressive stress fields could experience local tensile loading, and if so, whether thermally activated growth of such cracks might explain the observed strength behaviour. In Fig. 9, a twin nucleated in Grain 1 by the applied compressive stress σ impinges upon the grain boundary, forming an axial microcrack (recall Fig. 7). If the grains are misoriented, so that their effective moduli (E') mismatch across the

*It was shown in detail in earlier work that twinning is the sole source of microfracture in this regime. Thus, the question of thermally activated microcrack nucleation is directly tied to that of concurrent twinning.

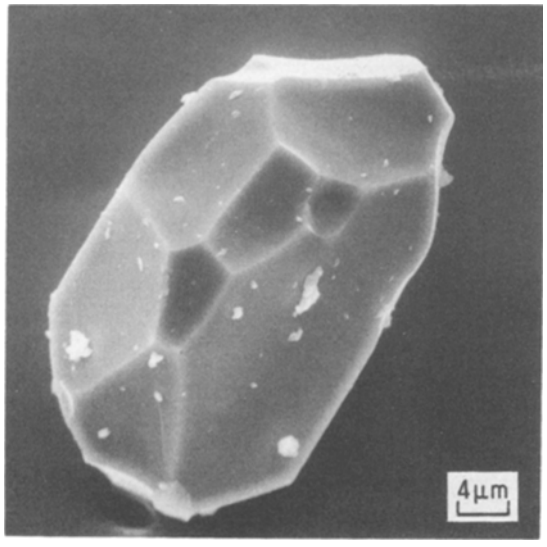

Figure 5 Particulate (crystallite) remnant of Al_2O_3 compressive failure, $\dot{\epsilon} = 2 \times 10^3\ sec^{-1}$, $T = 1800$ K.

boundary in such a way that the upper grain is compliant relative to the stiffer lower grain, then a local tensile stress will exist at the interface [7]. This stress will be proportional to the difference in ν/E', where ν is Poisson's ratio. Radial tension, therefore, will occur on the stiff side, reaching significant fractions of the applied compressive stress for only small differences in ν/E' between the two grains [8]. Other microscopic scenarios have also been suggested and observed which indicate the presence of tensile stresses across axial cracks in compressive specimens [9–11].

Under flexural (tensile) loading, the tensile strength σ_t of alumina, as for most ceramics, obeys a law of the form [12]

$$\sigma_t = B\dot{\epsilon}^{1/(1+n)}. \quad (1)$$

It turns out that n also is equal to the Region I power-law exponent in the empirical stress intensity (K_I)–Mode I crack velocity (V) relationship [12]

$$V = AK_I^n. \quad (2)$$

For Lucalox, room-temperature experiments of the latter sort show that $n = 52$ [5]. In the present compression experiments, it is possible to represent σ_c against $\dot{\epsilon}$ at room temperature (Fig. 2) by

$$\sigma_c = c\dot{\epsilon}^{1/(1+n')}, \quad (3)$$

in which case $n' = 51$. The excellent agreement between n' and n suggests, by analogy with the correlation of Equations 1 and 2 through n, that the strain-rate dependence of σ_c is controlled by thermally activated subcritical growth of Mode I axial cracks.

Further support for this proposition derives from consideration of the acoustic emission data. As shown in Fig. 3, the slope $S_2 = 10$ of the second stage of the dN/dt against compressive stress relationship is identical to the slope of the corresponding curve for the ground, pre-microcracked tensile specimen, in which the AE is known [5] to be caused by microcrack growth. Thus, Mode I microcrack extension again is implicated.

Finally, the apparent activation energy for the

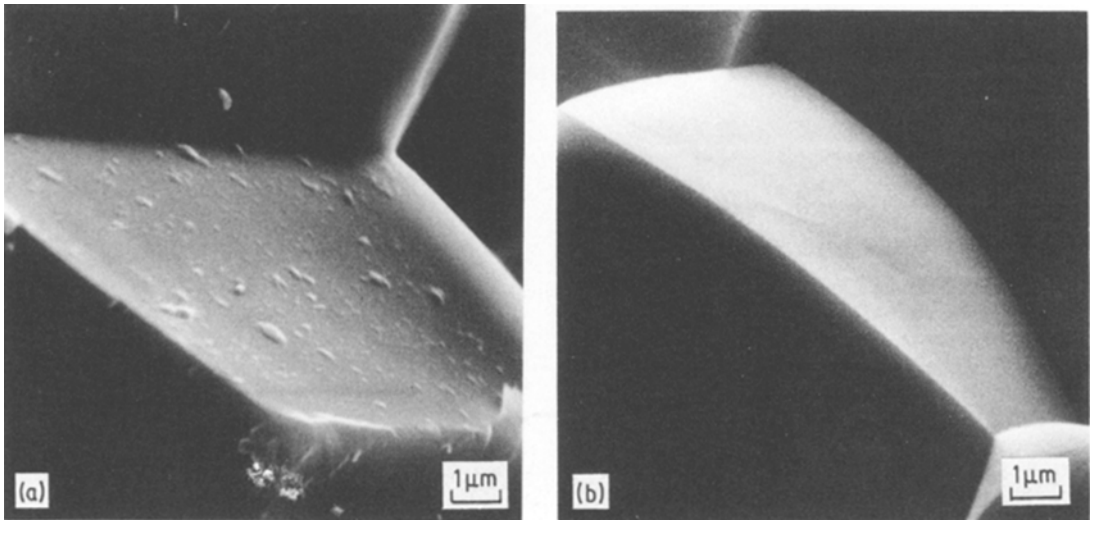

Figure 6 Al_2O_3 intergranular facets attending compressive failure. (a) Globular glassy phase, $\dot{\epsilon} = 2 \times 10^3\ sec^{-1}$, $T = 1800$ K. (b) Smooth facet, $\dot{\epsilon} = 7 \times 10^{-5}\ sec^{-1}$, $T = 900$ K.

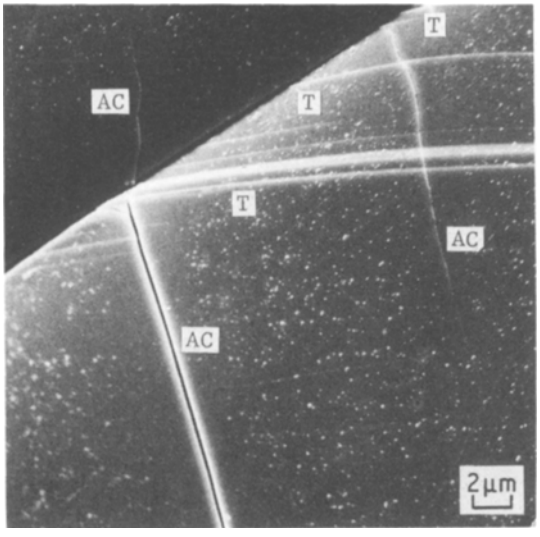

Figure 7 Crack initiation in Al_2O_3 under compressive loading, $T \lesssim 900$ K, compression axis vertical, axial cracks (AC), twins (T).

thermally activated process in question can be calculated using the data of Figs 1 and 2. For ceramic materials, one may usually write [13]

$$\dot{\epsilon} = \dot{\epsilon}_0 \exp\left[\frac{-H(\sigma_c)}{RT}\right], \tag{4}$$

where $\dot{\epsilon}_0$ is a frequency factor and $H(\sigma)$ is an activation energy. If we assume a linear relationship between H and σ_c, we see that

$$H = H_0 - V(\sigma_c - \sigma_0), \tag{5}$$

where V is an activation volume* and σ_0 is a threshold stress level. In this case, we will ignore σ_0, as it does not effect the ensuing calculation to a significant extent. Thus

$$H = H_0 - V\sigma_c. \tag{6}$$

At $T = 0$, $\sigma = \sigma_c^{(0)}$, hence

$$\sigma_c^{(0)} = \frac{H_0}{V}. \tag{7}$$

Similarly, at $T = T_1$, $\sigma_c = \sigma_c^{(1)}$, or

$$\sigma_c^{(1)} = \frac{H_0}{V} - \frac{RT_1}{V} \ln\left(\frac{\dot{\epsilon}_0}{\dot{\epsilon}_1}\right). \tag{8}$$

Combining Equations 7 and 8 to eliminate V yields

$$H_0 = \frac{RT_1\sigma_c^{(0)}}{\sigma_c^{(0)} - \sigma_c^{(1)}} \ln\left(\frac{\dot{\epsilon}_0}{\dot{\epsilon}_1}\right). \tag{9}$$

Using data shown in Fig. 2, we find that $H_0 \simeq 45$ kcal mol^{-1}. This is a relatively low activation energy, of the same order as values obtained for (ambient) slow crack tests in soda-lime glass (26 kcal mol^{-1}) [14] and silicon carbide (~30 kcal mol^{-1}) [15]. Equivalent data for Al_2O_3 are unavailable.

4.2. Region 2: $T \gtrsim 700$ K, $\dot{\epsilon} \gtrsim 10^3$ sec^{-1}

In this regime, fracture is no longer transgranular, and microcracks have much less tendency to form

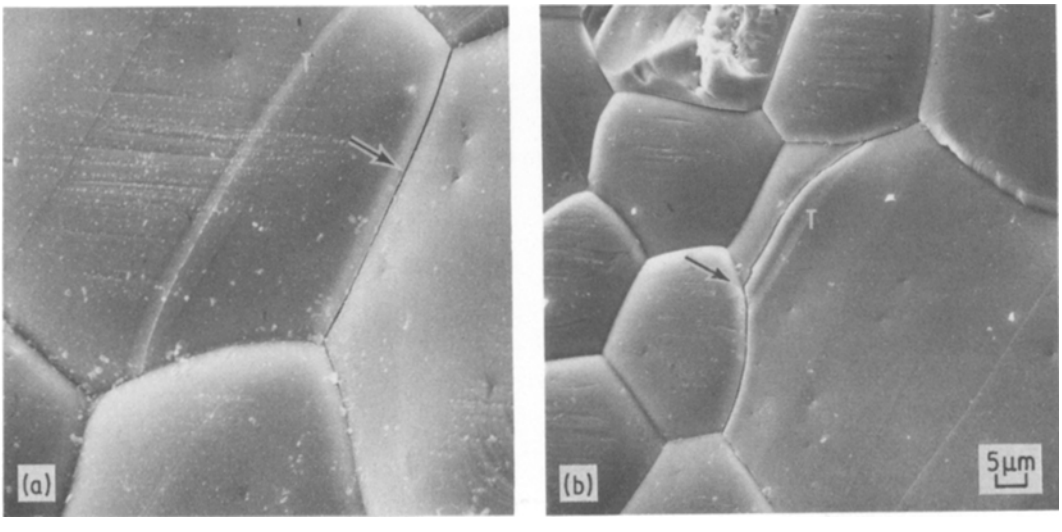

Figure 8 Crack initiation in Al_2O_3 under compressive loading, $T \gtrsim 900$ K, compression axis vertical. (a) Twinning (T) with no cracking; axial intergranular cracking (arrow); $T = 1560$ K. (b) Transition from twin (T)-nucleated transgranular (axial) cracking to intergranular (axial) cracking (arrow); $T = 1560$ K.

*This amounts to the assumption of a rectangular shaped thermal activation barrier; the author is not aware of data yielding any more precise statement of the barrier shape for thermally activated crack growth in Al_2O_3.

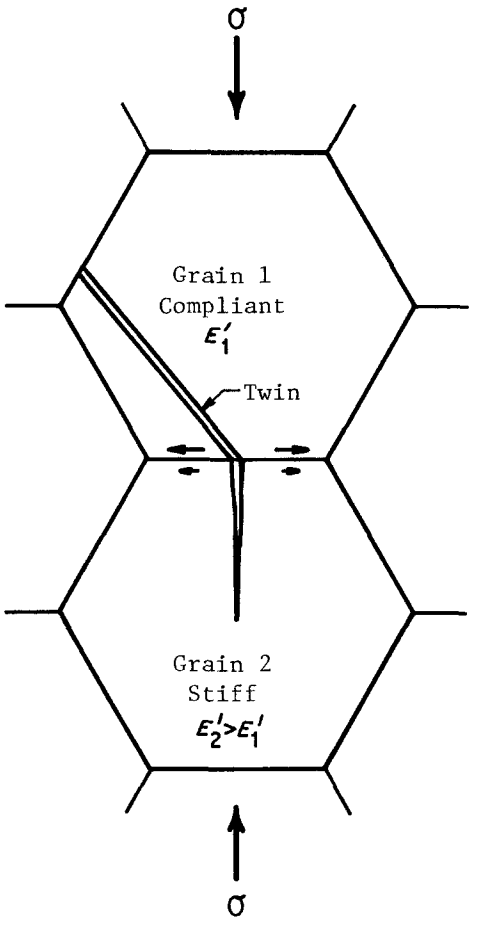

Figure 9 Conceptual sketch of resolution of applied compressive stress into local tensile stress normal to plane of axial microcrack. Interfacial arrows represent unequal elastic lateral displacements in the two grains, producing local tensile stress field at the interface [7].

via twinning. For $T \gtrsim 1000\,\mathrm{K}$, fracture is almost entirely intergranular, and apparently related to flow (cavitation) in a thin grain-boundary phase. The nature of the latter phase is unclear, despite a great deal of recent surface chemistry work [16–19] on Lucalox aimed at establishing its grain-boundary chemistry. Based on Auger electron spectroscopy, the only elements present in significant concentrations at the boundaries seem to be aluminium, oxygen, and calcium although Si, which is difficult to detect, may be present in small quantities [20]. The presence of Si in addition to the other elements detected could account for a low melting point ($T_{mp} \lesssim 1500\,\mathrm{K}$) glass phase. This point requires further study.

Clearly, however, a grain-boundary phase is present, and it is possible to show that cavitation in it is compatible with the observed $\sigma_c(T, \dot{\epsilon})$ dependence. In particular, Evans and Rana [21] have recently developed a statistical model of high-temperature ceramic failure through viscous growth of cavities in a thin grain-boundary phase. Although the model is derived in terms of constant stress creep experiments, i.e. creep lifetime, it can be used to estimate approximate time to failure for constant strain-rate experiments as well.

For example, the most extreme test of the model would be to predict the results of the pressure bar experiments, where the strain rates are approximately nine orders of magnitude higher than conventional creep rates. Let us consider the results of pressure bar tests at 1800 K, for which the compressive failure strength is $2650\,\mathrm{MN\,m^{-2}}$. The actual time to failure is given by

$$t_f = \sigma_c / E\dot{e}, \qquad (10)$$

where E is the modulus of elasticity. In this case, E is reduced by the elevated temperature [22] to $\sim 194\,\mathrm{GN\,m^{-2}}$, and with $\dot{e} \sim 10^3\,\mathrm{sec^{-1}}$, $t_f \approx 14\,\mu\mathrm{sec}$.

According to Evans and Rana, in a material containing a continuous second phase, cavitation should occur primarily within the second phase by viscous deformation. For high-strength ceramics at reasonably high applied stress levels, the time t_p for the formation of facet-sized cavities can be approximated by [21]

$$t_p \approx 0.15(\eta_0/\sigma_\infty)(l/\delta_0)^2 \exp(Q_\eta/RT), \qquad (11)$$

where η_0 is a constant, σ_∞ is the applied stress, l is the mean dimension of a facet, $2\delta_0$ is the initial thickness of the viscous phase, and Q_η is the activation energy for viscous flow. If we assume that the compressive failure event corresponds to the (essentially) instantaneous coalescence of such microcrack cavities, then we can roughly equate t_p with t_f. It is further assumed that the cavities form on axially oriented grain-boundary facets, due to resolved tensile stresses.

To determine whether this is reasonable, it is necessary to evaluate Equation 11 using the appropriate parameters. The average compressive stress during the course of the constant strain-rate test is $\sigma_c/2$; if the average tensile stress resolved across an axially oriented facet is assumed to be approximately half of the latter, then $\sigma_\infty \approx 660\,\mathrm{MN\,m^{-2}}$. The average facet dimension is $\sim 25\,\mu\mathrm{m}$, and a reasonable estimate for the film thickness δ_0 is $\sim 5\,\mathrm{nm}$ [21]. Based on tensile rupture experiments carried out by Walles [23] on Al_2O_3 fibres, Evans

and Rana determined that $\eta_0(l/\delta_0)^2 \sim 10^6$ poise. Using the preceding values for l and δ_0 in this relationship yields $\eta_0 \sim 10^{-2}$ poise. Finally, Q_η can be calculated from Fig. 2 using Equation 9 (setting $Q_\eta = H_0$), which provides an activation energy of 134 kcal mol^{-1}. This value shows reasonable agreement with that found by Walles [23], i.e. 115 kcal mol^{-1}. Incorporation of these numerical terms into Equation 11 yields a predicted failure time (for $\dot{\epsilon} \sim 10^3\,\text{sec}^{-1}$, $T = 1800$ K) of $\sim 29\,\mu$sec. Considering the approximations involved, agreement with the actual failure time of $\sim 14\,\mu$sec is considered good.*

4.3. Region 3: $\dot{\epsilon} \gtrsim 10^3\,\text{sec}^{-1}$

A sudden increase in the dependence of strength upon strain rate at high loading rates is an effect which has been noted recently for several types of rock [24], as well as for SiC [2]. In the latter case, the enhanced strain-rate dependence showed up in Hopkinson bar experiments, with the break occurring at $\dot{\epsilon} \sim 10^2\,\text{sec}^{-1}$. Thus, the existence of region 3 shown in Fig. 2, i.e. the departure of the Sandia data from the present experimental results, is considered to represent a real physical phenomenon.

In a recent series of papers, Grady and his colleagues [24–27] have addressed this behaviour as it pertains to rocks, developing a formalism for treating the rate dependence of fracture and fragmentation which is based upon inertial effects associated with the finite activation and growth times of the inherent flaw structure. One of the principal predictions of this analysis is that for situations in which dynamics (as opposed to subcritical, thermally activated mechanisms) are controlling fracture, strength should be proportional (approximately) to $\dot{\epsilon}^{1/3}$ [24]. In the present case, Fig. 2 shows that in region 3, $\sigma_c \propto \dot{\epsilon}^{0.27}$, in reasonable agreement with the crack inertia concept, particularly considering that the model has been formulated for tensile loading.

It is possible to analyse this concept further. As pointed out by Grady and Kipp [25], crack activation in general, i.e. static or dynamic, can be considered to be governed by a Weibull distribution of the form

$$N = k\epsilon^m, \tag{12}$$

where N is the number of flaws which will activate at or below a tensile strain level ϵ, and k and m are distribution fracture parameters. Further, it was shown that the static mean (tensile) fracture stress can be written as

$$\bar{\sigma}_M = I_m E(kV)^{-1/m}, \tag{13}$$

where I_m is a constant and V is the specimen volume.

It turns out that k and m are also critical parameters in relationships derived by Grady and Kip [25] for dynamic fracture strength and fragment size L_M in the high loading rate, flaw inertia-controlled regime. By using these relationships in conjunction with measured dynamic σ_c and L_M values, k and m can be established, and used in Equation 13 to predict the static tensile fracture strength. Comparison of the latter with $\bar{\sigma}_M$ found experimentally then serves as an indirect test of the applicability of the crack inertia† concept.

At compressive fracture coalescence, fracture surfaces consisting of axially oriented microcracks will form the sides of fragments having a mean size [25]

$$L_M = \frac{6C_g}{m+2}\alpha^{-[1/(m+3)]}\dot{\epsilon}^{-(m/m+3)}, \tag{14}$$

where C_g is the average velocity at which cracks activated under the applied load grow, and α is given by

$$\alpha = \frac{8\pi C_g^3 k}{(m+1)(m+2)(m+3)}. \tag{15}$$

The dependence of fracture stress σ_M upon strain rate is given by

$$\sigma_M = E(m+3)(m+4)^{-(m+4)/(m+3)} \times \alpha^{-[1/(m+3)]}\dot{\epsilon}^{3/(m+3)}. \tag{16}$$

In the present case, we equate σ_M with the compressive failure stress σ_c, for which we have already observed $\sigma_c \alpha \dot{\epsilon}^{0.27}$. Thus, from Equation 16, $3/(m+3) = 0.27$, hence $m \approx 8$.

The parameter k is obtained by substituting Equation 15 into Equation 14 and solving for k, using appropriate values for the remaining terms. Fragments generated in the Hopkinson bar experiments, in which $\dot{\epsilon} = 10^3\,\text{sec}^{-1}$, were examined in the SEM, and determined to have an average dimension of $L_M \approx 200\,\mu$m. With $m = 8$, $\dot{\epsilon} = 2 \times 10^3\,\text{sec}^{-1}$, and assuming that C_g is approximately 10% of the sound velocity in the material, i.e.

*Comparison of t_p with t_f for the lower $\dot{\epsilon}$ nearer classical creep rates showed similar relative agreement.

†Strictly speaking, one means *material* inertia, since a crack has no mass. However, this is not a material property effect, like the thermally activated processes discussed earlier, but simply a consequence of a crack growing rapidly in any real, inertial material.

$C_g \approx 1 \times 10^3\,\mathrm{m\,sec^{-1}}$, k is found to be 3.5×10^{36} $\mathrm{m^{-3}}$.

Using the preceding values for k and m, $\bar{\sigma}_M$ can be calculated. For $m = 8$, I_m has been estimated as ≈ 1.0. Static tensile tests of Lucalox were previously [3] carried out in three-point bending, for which it is estimated that the stressed volume was approximately $6 \times 10^{-9}\,\mathrm{m^3}$. Thus, Equation 13 yields a calculated $\bar{\sigma}_M$ of $120\,\mathrm{MN\,m^{-2}}$, which, considering the approximations involved, compares reasonably well with the experimental value of $215\,\mathrm{MN\,m^{-2}}$ [3].

5. Discussion

It is concluded that compressive failure in Al_2O_3 can be described in terms of three variants of axial cracks growing under the influence of local tensile stress fields. One process involves thermally activated growth of subcritical, transgranular cracks, nucleated athermally by twins formed over a characteristic stress range. At higher temperature, the efficiency of the twins as crack initiators drops as their character is altered through a thickening process. Concurrently, the grain boundaries become sites of microcrack initiation through thermally activated viscous flow and cavitation. Since the nucleating twins lose some of their effectiveness at temperatures below which the grain boundaries are yet unable to flow easily, there is an apparent strengthening effect in this intermediate temperature range (600 to 900 K, Fig. 1).

Finally, for $T \lesssim 500\,\mathrm{K}$ (and possibly for much higher temperatures*) failure at impact-loading rates is controlled by a crack velocity (i.e. non-thermally activated), highly strain rate-sensitive process. The quantitative predictions of analytical models based upon each of these concepts are fulfilled by the results of the compressive experiments.

The results of this study have strongly implicated a critical role for tensile axial cracks in compressive failure. This concept is supported by a large recent body of work in the rock mechanics literature, in which dilatancy of compressive specimens has been explained in terms of the tensile opening of axial microcracks [28]. Recent observations by Kranz [9] have, in fact, confirmed the tensile character of compression-induced axial microcracks in granite. Finally, the writer has shown [29] that the strain-rate dependence of compressive strength in limestone (which fails in a manner similar to granite) can be explained quantitatively by the same tensile microcrack growth concepts invoked in the present paper.

Aluminium oxide is usually considered to be a model brittle material; aside from its twinning propensity, its mechanical behaviour is similar to that of other strong ceramics. There is thus good reason to believe that the several compressive failure regimes outlined here for Al_2O_3 should be observed in other engineering ceramics (and many rocks) as well. In the case of SiC and Si_3N_4, for instance, crack initiation should occur at the sharp-edged micropores characteristic of their microstructures, and such initiation probably would be athermal. Observation of compressive crack nucleation in SiC already suggests [30] that the pores do indeed nucleate axial cracks.

On the other hand, for materials like MgO, which can deform plastically at relatively low temperatures and thereby nucleate slip-band cracks, there probably is a thermally activated crack nucleation mechanism superimposed upon that of subcritical crack growth. This would complicate the failure analysis, which was simplified in the present case by the absence of such considerations. Similarly, ceramics such as sintered α-SiC and NC-350 silicon nitride apparently have no viscous grain-boundary film. In this case, high-temperature failure would proceed by a mechanism such as grain-boundary diffusion, for example, rather than viscous-phase cavitation; this obviously would alter the failure criterion, and yield a different functional dependence for crack growth.

For a given brittle ceramic material, quantitative *changes* in its compressive strength can be accounted for through the thermally activated and inertial models of tensile crack extension which have been discussed. However, the *general* strength level of the ceramic will depend upon its initial flaw distribution and character (pores, their relative smoothness, microcracks, minor second phases, etc.), and the ease with which flaws are produced (twinning, slip, phase transformation), since it is these crack nucleation factors which de-

*There is no obvious reason why the crack inertia effect should not prevail at elevated temperatures as well. However, verification of this point will require high-temperature failure tests at rates in excess of those generated in the Hopkinson pressure bar. If the mechanism is operative at elevated temperatures, the curve in Fig. 2 for $\dot{\epsilon} = 10^6$ and $10^9\,\mathrm{s^{-1}}$ would move to higher stresses.

termine the stress level and initial size at which axial microcracks are able to begin to grow. This suggests that specific attention should be directed at understanding and characterizing these nucleation processes in various ceramics.

Acknowledgements

The writer is grateful to D. L. Davidson and U. S. Lindholm for their helpful comments, to H. Muehlenhaupt for his excellent experimental work in performing the compression experiments, and to M. Luckey for his careful specimen preparation. Support of the Office of Naval Research under Contract No. N00014-75-C-0668 is greatly appreciated.

References

1. J. LANKFORD, *J. Mater. Sci.* **12** (1977) 2195.
2. J. LANKFORD and D. L. DAVIDSON, Proceedings of the Third International Conference on the Mechanical Behaviour of Materials, Vol. 3 (University of Waterloo Press, Ontario, 1979) p. 35.
3. J. LANKFORD, *J. Mater. Sci.* **13** (1978) 351.
4. D. E. MUNSON and R. J. LAWRENCE, *J. Appl. Phys.* **50** (1979) 6272.
5. A. G. EVANS, M. LINZER and L. R. RUSSELL, *Mater. Sci. Eng.* **15** (1974) 253.
6. O. JOHARI and N. M. PARIKH, in "Fracture Mechanics of Ceramics", Vol. 1, edited by R. C. Bradt, D. P. H. Hasselman and F. F. Lange (Plenum Press, New York, 1974) p. 399.
7. P. TAPPONIER and W. F. BRACE, *Int. J. Roch Mech. Min. Sci. & Geomech. Abstr.* **13** (1976) 103.
8. B. T. BRADY, *Int. J. Rock Mech. Min. Sci.* 8 (1971) 357.
9. R. L. KRANZ, *Int. J. Roch Mech. Min. Sci. & Geomech. Abstr.* **16** (1979) 23.
10. E. G. BOMBOLAKIS, *Tektonophysics* **1** (1964) 343.
11. S. KOBAYASHI, *J. Soc. Mater. Sci. Jap.* **20** (1971) 164.
12. A. G. EVANS and S. M. WIEDERHORN, *Int. J. Fract.* **10** (1974) 379.
13. K. C. RADFORD and G. R. TERWILLIGER, *J. Amer. Ceram. Soc.* 58 (1975) 274.
14. A. G. EVANS, *J. Mater. Sci.* 7 (1972) 1137.
15. A. G. EVANS and F. F. LANGE, *ibid* **10** (1975) 1659.
16. H. L. MARCUS and M. E. FINE, *J. Amer. Ceram. Soc.* 55 (1972) 568.
17. W. C. JOHNSON and D. F. STEIN, *ibid* 58 (1975) 485.
18. W. C. JOHNSON, *Met. Trans. A* 8A (1977) 1413.
19. D. R. CLARKE, *J. Amer. Ceram. Soc.* **63** (1980) 339.
20. W. C. JOHNSON, private communication (1979).
21. A. G. EVANS and A. RANA, *Acta Met.* **28** (1980) 129.
22. J. B. WACHTMAN and D. G. LAM, Jr, *J. Amer. Ceram. Soc.* **42** (1959) 254.
23. K. F. A. WALLES, *Proc. Brit. Ceram. Soc.* **15** (1970) 157.
24. D. E. GRADY and J. LIPKIN, *Geophys. Res. Letters* 7 (1980) 255.
25. D. E. GRADY and M. E. KIPP, "Oil Shale Fracture and Fragmentation at High Rates of Loading", Sandia Report SAND-79-0563C (1979).
26. D. E. GRADY and R. E. HOLLENBACH, "Rate-Controlling Processes in the Brittle Failure of Rock", Sandia Report SAND-76-0659 (1977).
27. D. E. GRADY and M. E. KIPP, *Int. J. Rock Mech. Min. Sci. & Geophys. Abstr.* **16** (1979) 293.
28. W. JANNACH, *Int. J. Rock Mech. Min. Sci. & Geomech. Abstr.* **14** (1977) 209.
29. J. LANKFORD, to be published.
30. *Idem, J. Amer. Ceram. Soc.* **62** (1979) 310.

Received 11 September and accepted 10 November 1980.